Sodium-Ion Batteries | Hot Paper

DOI: 10.1002/ange.201404549

An Ultrastable Anode for Long-Life Room-Temperature Sodium-Ion Batteries**

Haijun Yu, Yang Ren, Dongdong Xiao, Shaohua Guo, Yanbei Zhu, Yumin Qian, Lin Gu, and Haoshen Zhou**

Abstract: *Sodium-ion batteries are important alternative energy storage devices that have recently come again into focus for the development of large-scale energy storage devices because sodium is an abundant and low-cost material. However, the development of electrode materials with long-term stability has remained a great challenge. A novel negative-electrode material, a P2-type layered oxide with the chemical composition $Na_{2/3}Co_{1/3}Ti_{2/3}O_2$, exhibits outstanding cycle stability (ca. 84.84 % capacity retention for 3000 cycles, very small decrease in the volume (0.046 %) after 500 cycles), good rate capability (ca. 41 % capacity retention at a discharge/charge rate of 10 C), and a usable reversible capacity of about 90 mAh g^{-1} with a safe average storage voltage of approximately 0.7 V in the sodium half-cell. This P2-type layered oxide is a promising anode material for sodium-ion batteries with a long cycle life and should greatly promote the development of room-temperature sodium-ion batteries.*

With increasing concerns regarding the depletion of fossil fuels, the development of methods to make use of green and sustainable energy has become more and more important. Therefore, large-scale energy storage devices have been introduced and developed quickly.[1] Recently, lithium-ion batteries (LIBs) have widely been used by the automotive industry and for partial energy storage devices for electrical grid systems.[1a] However, lithium is not considered to be an abundant element in the Earth's crust although it is widely distributed, and the limited availability of lithium has resulted in increasing material costs after the wide commercialization of LIBs.[1a,2]

In contrast, sodium is considered to be a low-cost material because of its abundance in the Earth's crust. Furthermore, sodium is incorporated by a "rocking-chair" reaction mechanism similar to that of lithium, and room-temperature rechargeable sodium-ion batteries (NIBs) are thus promising candidates for large-scale applications.[2b,c,3] Recent advances in the development of NIBs focused on the development of electrode materials, and the majority of the work done so far has been on the positive electrode materials. Various layered compounds, such as $Na_x[Fe_{1/2}Mn_{1/2}]O_2$,[2b] $NaNi_{0.5}Ti_{0.5}O_2$,[2c] and $Na_{1-x}Ni_yMn_zCo_{1-y-z}O_2$,[3a,e,g,h] polyanion-based $Na_3V_2(PO_4)_3$,[4] $Na_{1.5}VPO_{4.8}F_{0.7}$,[3l] $Na_2(Fe_xMn_{1-x})P_2O_7$,[3i,5] and $Na_3MnPO_4CO_3$,[3m] and Prussian blue[3n–p] have been used for the positive electrodes for NIBs. However, there have been considerably fewer studies on the use of sodium insertion materials as the negative electrodes of NIBs.[2a,3q,6] Although hard carbon materials have shown good electrochemical performance,[6a] more than half of the discharge capacity is distributed at a very low discharge plateau between 0 and 0.1 V versus Na^+/Na, which leads to serious safety concerns related to the possible formation of sodium dendrite and the associated thermal runaway because of the low melting point of sodium metal (97.7 °C).[3k,6a] Titanium-based intercalation compounds, which benefit from a safe and low redox potential (Ti^{3+}/Ti^{4+}) relative to the Na^+/Na redox potential, are another class of potential materials for the negative electrode of NIBs, and have been reported recently.[2a,6b] However, their cycle capability, which is closely related to the structure stability, is still not sufficient for the long-term operation of large-scale energy storage devices.

Herein, a novel titanium-based negative electrode material for NIBs, $Na_{2/3}Co_{1/3}Ti_{2/3}O_2$ (NCT), is prepared (see the Supporting Information) and used as the anode of NIBs for the first time. It exhibits a pure and ultrastable P2-type layered structure,[3a,7] which shows outstanding cycle stability (ca. 84.84 % capacity retention after 3000 cycles and a very

[*] Dr. H. J. Yu, S. H. Guo, Dr. Y. M. Qian, Prof. H. S. Zhou
Energy Technology Research Institute, National Institute of Advanced Industrial Science and Technology (AIST)
Tsukuba, 305-8568 (Japan)
E-mail: hs.zhou@aist.go.jp
Prof. H. S. Zhou
National Laboratory of Solid State Microstructures & Department of Energy Science and Engineering
Nanjing University, Nanjing 210093 (China)
Dr. Y. Ren
X-ray Science Division, Argonne National Laboratory
9700 South Cass Avenue, Argonne, IL 60439 (USA)
D. D. Xiao, Prof. L. Gu
Institute of Physics, Chinese Academy of Sciences
Beijing National Laboratory for Condensed Matter Physics
Beijing, 100190 (P. R. China)
E-mail: l.gu@iphy.ac.cn
Dr. Y. B. Zhu
National Metrology Institute of Japan, National Institute of Advanced Industrial Science and Technology
Tsukuba, 305-8568 (Japan)

[**] This work was partially supported by the Funding Program for World-Leading Innovative R&D on Science and Technology (FIRST Program). We thank Dr. Matthew Suchomel for help with the high-resolution synchrotron powder diffraction measurements, and Dr. Zhiping Song for help with the cover picture design. The use of the Advanced Photon Source at Argonne National Laboratory was supported by the U. S. Department of Energy, Office of Science, Office of Basic Energy Sciences (DE-AC02-06CH11357).

Supporting information for this article is available on the WWW under http://dx.doi.org/10.1002/anie.201404549.

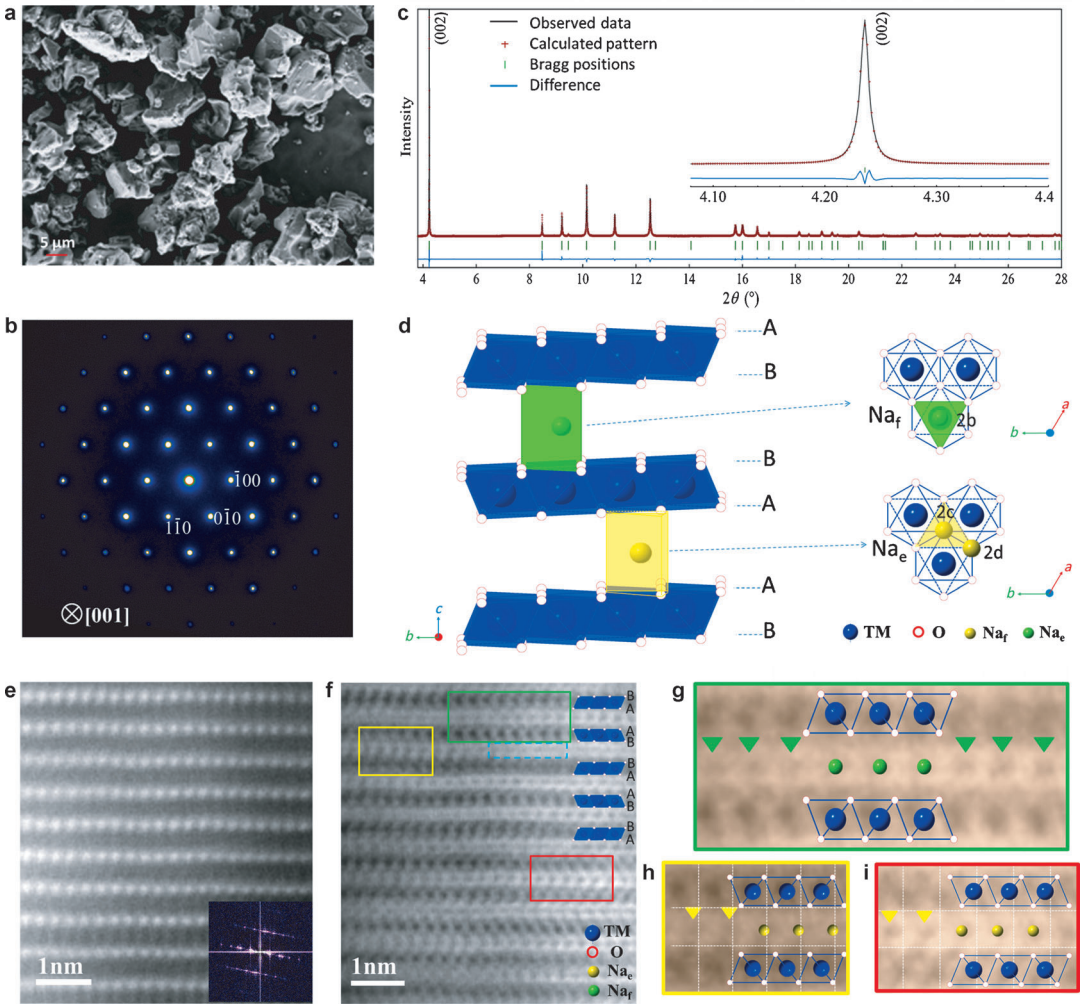

Figure 1. a) SEM and b) SAED images of as-prepared P2-NCT. c) HR-SXRD patterns of the P2-NCT material and Rietveld refinement. The inset shows the enlarged (002) diffraction line of the P2-NCT material. d) Schematic representation of the P2-NCT crystal structure and local sodium environments. A and B represent the two different oxygen layers. e) HAADF and f) ABF STEM images of the pristine P2-NCT material projected along the [110] direction. Inset in Figure 1 e: FFT pattern. Inset in Figure 1 f, top-right corner: typical transition-metal octahedra in a P2-type structure. g) Enlarged image of the green rectangle in Figure 1 f, showing the Na^+ occupancy of Na_f positions. h, i) Enlarged images of the yellow and red rectangles in Figure 1 f, showing the Na^+ occupancies of the Na_e positions with 2c and 2d Wyckoff sites, respectively. The dotted blue lines in Figure 1 f represent Na^+ vacancies.

small volume contraction of 0.046 % after 500 cycles), good rate capability (ca. 41 % capacity retention at a discharge/charge rate of 10 C), and a usable reversible capacity of approximately 90 mAh g^{-1} with a safe average storage voltage of about 0.7 V in the sodium half-cell. This novel P2-type layered oxide is a most promising anode material for NIBs with a long cycle life and extremely attractive for large-scale energy storage devices.

The morphology of as-prepared P2-NCT was analyzed by scanning electron microscopy (SEM) and found to be irregular, with particle sizes of 10–15 μm (Figure 1 a). Composition analysis by inductively coupled plasma mass spectrometry (ICP-MS) on the pristine material revealed that the actual chemical formula of P2-NCT is $Na_{0.67}Co_{0.31}Ti_{0.65}O_2$, which is consistent with our intended composition ($Na_{0.67}Co_{0.33}Ti_{0.67}O_2$). The scanning area electron diffraction (SAED) pattern of P2-NCT projected along the [001] direction corresponds to a diffraction pattern typical for a pure hexagonal lattice (Figure 1 b). The high-resolution synchrotron X-ray diffraction (HR-SXRD) pattern of P2-NCT is shown in Figure 1 c, and it is clear that all diffraction lines can be well indexed to a hexagonal lattice with the *P*63/*mmc* space group, which is isostructural with P2-type $Na_{2/3}CoO_2$, and in agreement with the SAED results. Rietveld refinement of the HR-SXRD pattern using the RIETAN-FP program[8] gave refined lattice parameters of $a = b =$ 2.96552(4) Å, $c = 11.1735(1)$ Å, and $V = 85.098(1)$ Å^3 with a reliability index (R_{wp}) of 9.447 %. Therefore, the calculated HR-SXRD patterns are in good agreement with the experimental data, which is also corroborated by the enlarged (002) diffraction line shown in the inset of Figure 1 c, indicating that a material with a pure P2-type phase with good crystallinity has been obtained.

The ABBA stacking of the oxygen layers and two typical Na^+ positions in P2-NCT are shown in a schematic representation of P2-NCT (Figure 1 d). In this structure, the Co and Ti ions occupy the 2a Wyckoff sites, and all of the Na^+ ions occupy trigonal prismatic sites, but with different next-nearest neighbors. As shown in the schematic representation of the local Na^+ environment (Figure 1 d, right), Na^+ prisms located at Na_f positions with 2b Wyckoff sites share two faces with the upper and lower $(CoTi)O_6$ octahedra, while Na^+ prisms located at Na_e positions with 2c and 2d Wyckoff sites share edges with the six $(CoTi)O_6$ octahedra. The Na^+ occupancies of these two positions (Na_f and Na_e) are 0.208 (2) and 0.461 (2), respectively. The local structure of P2-NCT was analyzed with atomic resolution by annular bright field (ABF) and high-angle annular dark field (HAADF) scanning transmission electron microscopy (STEM; Figure 1 e–i).

These images are consistent with the P2-NCT structure projected along the [110] direction. The bright-dot contrast in the HAADF STEM images (Figure 1 e) and the dark-dot contrast in ABF STEM images (Figure 1 f) reveal the transition-metal (Co and Ti) atom column positions; the faint, but distinct dark-dot contrast in the interlayer positions of ABF STEM (Figure 1 f) corresponds to the sodium and oxygen atom column positions in the P2-NCT structure. It is obvious that the oxygen arrangement along the *c* axis corresponds to a typical P2-type structure and overlaps well with the $(CoTi)O_6$ octahedra inserted in the top-right corner (Figure 1 f). Na^+ ions at Na_f (2b Wyckoff sites) and Na_e (2c/2d Wyckoff sites) positions are marked with green and yellow/red rectangles in Figure 1 f; enlarged images of these regions are shown in Figure 1 g, h, and i, respectively. The validity of the sodium ion occupancy at the Na_f and Na_e positions is clearly demonstrated by the inserted crystal structure models. These results are consistent with the HR-SXRD analysis. Furthermore, it follows that Na^+ ions do not simultaneously occupy nearest-neighboring positions of the Na_f and Na_e sites in the P2-NCT structure, which is mainly due to electrostatic repulsion and the distance between these sites, which is smaller than the Na^+ ionic radius.[3a,9] It should be mentioned that Na^+ ions in Na_xTMO_2 (TM = transitional metal) layered materials that occupy two different positions (Na_e and Na_f) were thus observed and directly distinguished for the first time. Furthermore, it was confirmed for the first time that Na^+ ions occupy both 2c and 2d Wyckoff sites, revealing complex Na^+ ordering in the P2-NCT material.

The electrochemical performance of the composite electrode in sodium half-cells was evaluated. The first cycle of this composite electrode in voltage ranges of 0–3.5 V, 0–2.5 V, and 0.15–2.5 V resulted in a large irreversible capacity (Supporting Information, Figure S2), which is caused largely by the carbon additive.[6c,d] Actually, lots of Na^+ ions can be inserted into the carbon additive during the first discharge process, whereas only few Na^+ ions can be extracted during the first charge process, and the influence of the carbon additive on the sodium storage can be neglected during subsequent cycling (Figure S3). Furthermore, the formation of a solid electrolyte interface (SEI) film on the surface of P2-NCT could also contribute to the irreversibility of the initial few cycles,[2a,6d] which was confirmed by the observation of the SEI film by HR-TEM (Figure S4). After three cycles, the Na^+ insertion/extraction processes are not influenced by side reactions in all of the tested voltage ranges (0–3.5 V, 0–2.5 V, and 0.15–2.5 V), and reversible capacities of approximately 105, 100, and 90 $mAh\,g^{-1}$, respectively, were measured for the fourth cycle (Figure 2 a).

The variations of the voltage relative to the Na^+ insertion/extraction processes are smooth during the whole discharge/charge plateaus, especially for a voltage range of 0.15–2.5 V. It is very different from the complex and multiple plateaus observed for most reported electrode materials for NIBs,[2b,3a,g,j,m] indicating good structure stability and no phase transitions during Na^+ insertion/extraction into/from the P2-NCT electrode material. The small charge/discharge plateaus located at a low voltage of 0.1 V, which are associated with voltage ranges of 0–3.5 V and 0–2.5 V, resulted from side reactions of acetylene black as there is an obvious and strong redox couple below 0.15 V (Figure S3 b). To diminish the influence of the side reactions and evaluate the overall electrochemical performance of P2-NCT, a voltage of 0.15–2.5 V was chosen for the following investigations on rate capability and cycle stability. To activate as many Na^+ ions in the P2-NCT structure as possible, all of the electrodes for cycle and rate performance evaluation were first discharged/charged three times at a low current density of 20 $mA\,g^{-1}$ within the voltage range of 0.15–2.5 V. This voltage range was found to lead to the best cycle performance by a comparison of the electrochemical performances at this voltage and at 0–3.5 V and 0–2.5 V (Figure S5–S7).

The rate performance of the P2-NCT electrode is shown in Figure 2 b. The sample displayed a reversible capacity of 79 % at a rate of 1 C (100 $mA\,g^{-1}$), and the capacity retention could reach 41 % even at a current density of 10 C (1000 $mA\,g^{-1}$). It should be noted that the fraction of conductive additive in these electrodes is only 15 %, which is a typical value for investigating the electrochemical performance of electrode materials for LIBs,[10] and it should be possible to further improve the rate performance of P2-NCT through a surface treatment (e.g., carbon coating). This good rate performance of the P2-NCT electrode should enable its utilization in energy storage devices for surge wind and solar power, which both suffer from natural unpredictability and intermittency.

The cycle stability of the P2-NCT electrode materials in a sodium half-cell at a constant current density of 1 C is shown in Figure 2 c. All of the charge/discharge and dQ/dV curves (from the 4th to the 203rd cycle) almost overlap, and there is no obvious degradation of the reversible capacity after 200 cycles of Na^+ insertion/extraction (Figure S7), confirming the good cycle performance.

Inspired by the stable cycling and good rate capability, long-term cycling and the related Coulombic efficiency of this material were also studied at higher current densities (Figure 2 d). Capacity retentions of 95.67 % and 84.84 % were measured even after 1000 and 3000 cycles of Na^+ insertion/extraction at constant current densities of 2 C (200 $mA\,g^{-1}$) and 5 C (500 $mA\,g^{-1}$), respectively, and capacity-decay rates only amounted to approximately 0.005 % per cycle. Therefore, to the best of our knowledge, this material exhibits the

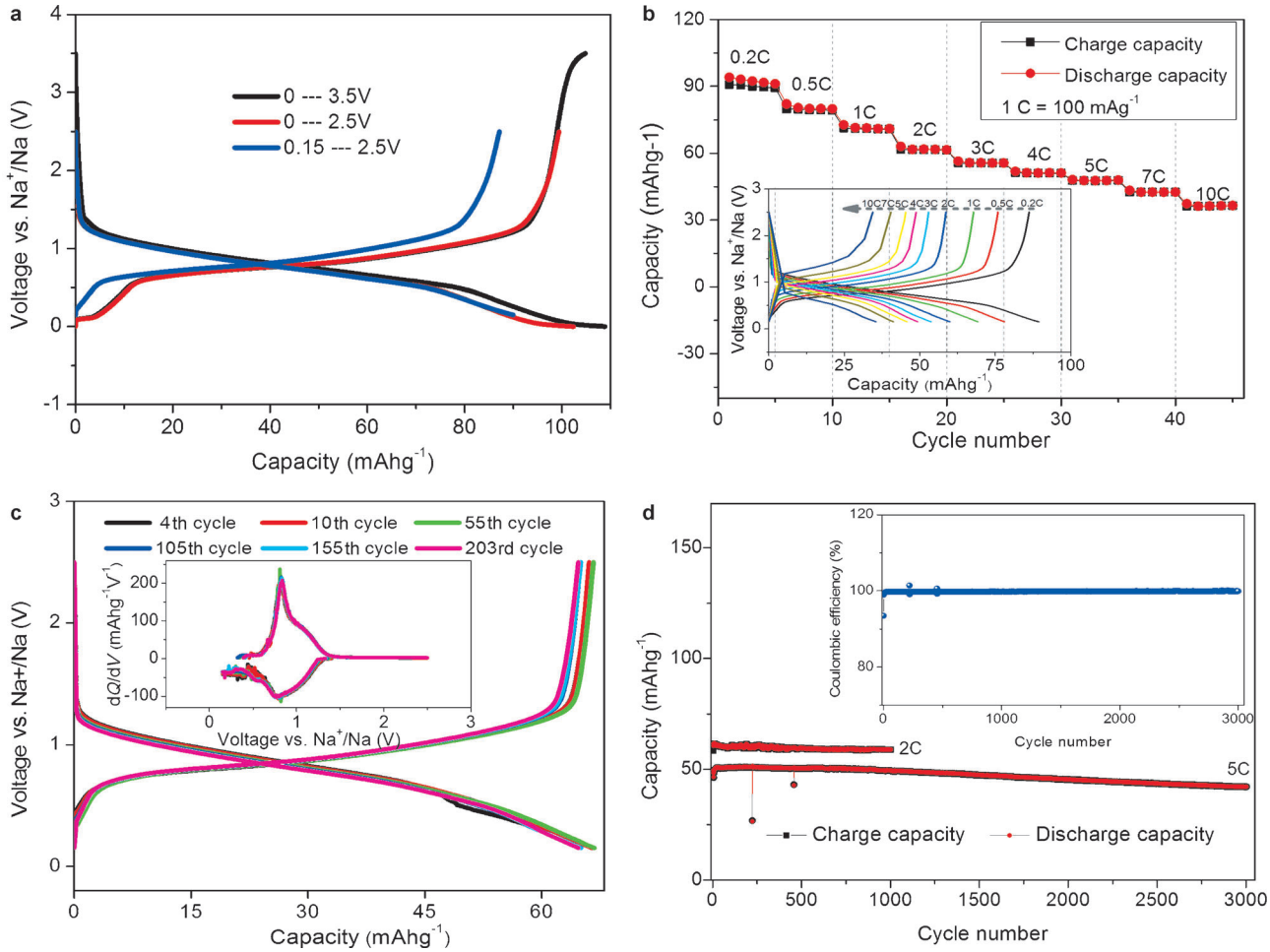

Figure 2. Electrochemical performance of the P2-NCT electrodes in sodium half-cells. a) The galvanostatic discharge/charge curves of the fourth cycle at a current rate of 0.2 C (20 mA g^{-1}) and voltage ranges of 0–3.5 V, 0–2.5 V, and 0.15–2.5 V. b) Rate capability at various current rates. Inset: galvanostatic discharge/charge curves at different rates. c) The 4th, 10th, 55th, 105th, and 203rd discharge/charge curves at a current rate of 1 C (100 mA g^{-1}). Inset: reversible variation of the dQ/dV curves within 200 cycles. d) Long-term cycle stabilities at current rates of 2 C (200 mA g^{-1}) and 5 C (500 mA g^{-1}). Inset: Coulombic efficiency of the P2-NCT electrode over 3000 cycles.

best cycling performance among all of the reported negative-electrode materials for NIBs.

More importantly, all of the Coulombic efficiencies (except for the initial and a few special cycles) of this electrode material were measured to be about 99.9%, which is extremely close to the ideal value of 100%. The appealing electrochemical performance of P2-NCT, which features excellent long-term cycle stability and Coulombic efficiency, can prompt the use of NIBs for large-scale energy-storage devices. To elucidate the sodium storage mechanism and reveal the reasons for the good cycle life of the P2-NCT electrode, ex situ HR-SXRD experiments on the electrode materials were conducted during cycling. The HR-SXRD patterns of the pristine state (sample 1), the state discharged at 0.15 V (sample 2), the state charged at 2.5 V in the first cycle (sample 3), and the state discharged at 0.15 V in the 500th cycle (sample 4) of Na^+ insertion/extraction are shown in Figure 3a. No obvious changes were observed for all of the diffraction lines of the P2-NCT electrode materials during the first cycle, and even after 500 cycles of Na^+ insertion/extraction. In particular, no obvious new peaks could be observed after the 1st and the 500th cycle; the structure thus corresponds to a single pure P2 phase, indicating excellent structure stability for the P2-NCT electrode under long-time operation with electrochemical Na^+ insertion/extraction. Moreover, all of the shapes of the enlarged (002) diffraction lines in Figure 3b are in good symmetry for samples 1 to 4, and broad features were not observed, indicating that only a single phase existed even at the end of the process of inserting/extracting Na^+ ions into/from the P2-NCT crystal structure.

Rietveld refinement of the HR-SXRD patterns that were obtained during cycling was also performed. The amount of Co and Ti in these electrode materials was determined by inductively coupled plasma atomic emission spectroscopy (ICP-AES), whereas the sodium content was determined by measuring the reversible electrochemical capacity in the voltage range of 0.15–2.5 V, assuming that all charges were consumed by the sodium extraction/insertion process without any side reactions, such as electrolyte decomposition.[11]

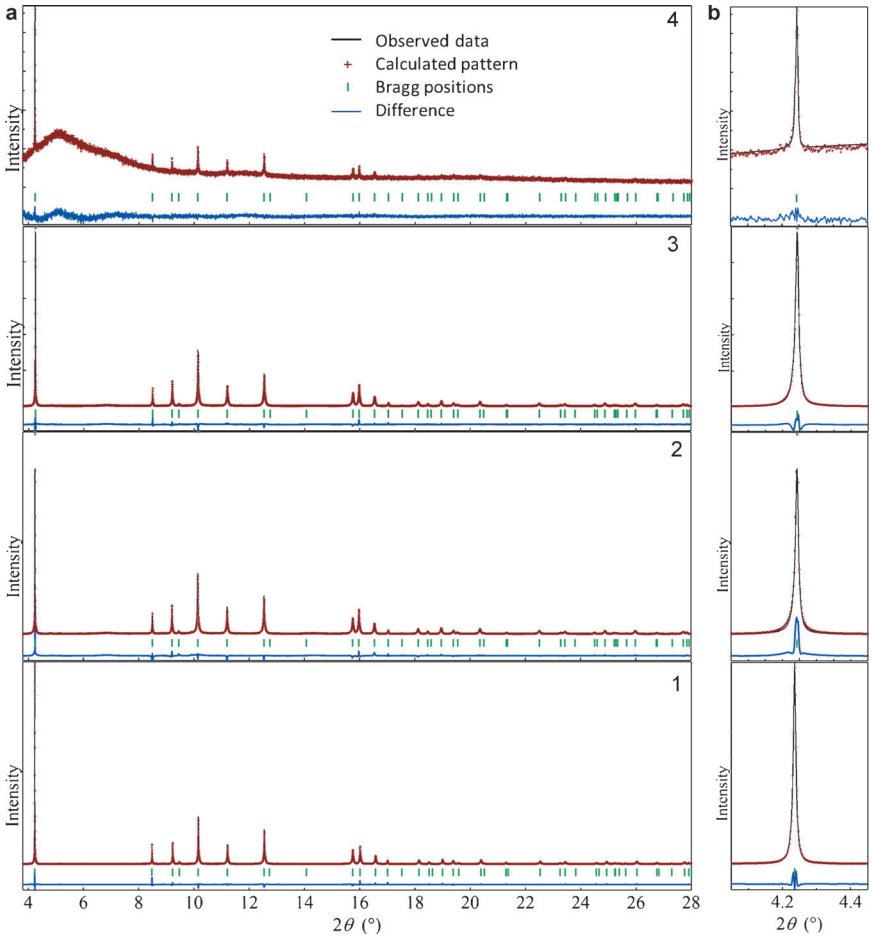

Figure 3. Ex situ structure evolution of the P2-NCT electrode during electrochemical cycling between 0.15 and 2.5 V. a) Ex situ HR-SXRD patterns and Rietveld refinement of the P2-NCT electrodes at different states. b) Enlarged (002) diffraction lines of Figure 3 a.

Owing to the strong correlation between atom occupancy and isotropic displacement (B) parameters in Rietveld analysis, all of the B parameters for the Na, Co, Ti, and O atoms were restricted to the values obtained by the refinement for pristine P2-NCT (Table 1 and Table S1). The peak profile, lattice parameters, sodium occupancy fractions at the Na_f (2b Wyckoff sites) and Na_e (2c Wyckoff sites) positions, and oxygen positional parameters were simultaneously refined under this restriction.

In Figure 3 a, it can be seen that all of the calculated X-ray diffraction patterns are in good agreement with the experimental data when only the P2-type single-phase model is used, which is also confirmed by the enlarged calculated (002) diffraction lines in Figure 3 b and the reliability indexes (R_{wp}, R_p, and S) in Table 1. The observations based on the evolution of the ex situ HR-SXRD patterns and the smooth discharge/charge curves in Figure 2 a imply a possible solid–solution mechanism for sodium storage of P2-NCT. A variation of the lattice parameters reveals that the c axis is contracted by 0.17 %, while the a (b) axis is expanded by 0.23 % after Na^+ insertion into the pristine material (samples 1 and 2; Table 1). Thus, the volume of the crystal structure of P2-NCT is expanded by only 0.28 % in this process. These variations of the c and a (b) axes and the volume are far smaller than those of other electrode materials for NIBs, indicating very small structural changes and good zero-strain character. Interestingly, no obvious changes in the lengths of the c axis and the a (b) axis were detected during the following Na^+ ion extraction process (sample 2 to 3), and the volume of the crystal structure only decreased by 0.0082 %.

The unmatched lattice-parameter variation of the first cycle suggests that the tiny structural change is irreversible. If

Table 1: Crystal parameters refined by the Rietveld method on the HR-SXRD patterns of pristine P2-NCT and electrochemically cycled samples (2, 3, and 4).

		Pristine (1)	Discharged, 0.15 V (2)	Charged, 2.5 V (3)	Discharged, 0.15 V, after 500 cycles (4)
composition		$Na_{0.67}Co_{0.31}Ti_{0.65}O_2$	$NaCo_{0.33}Ti_{0.66}O_2$	$Na_{0.67}Co_{0.32}Ti_{0.68}O_2$	$Na_{0.96}Co_{0.32}Ti_{0.68}O_2$
space group		*P*63/*mmc*	*P*63/*mmc*	*P*63/*mmc*	*P*63/*mmc*
Cell parameters					
lattice constants [Å]	*a*	2.96552 (4)	2.9722 (1)	2.97211 (7)	2.9721 (3)
	c	11.1735 (1)	11.1545 (2)	11.1545 (2)	11.1512 (9)
unit cell volume [Å^3]	*V*	85.098 (1)	85.339 (4)	85.332 (3)	85.30 (1)
Na_e (2c site)	Na [g]	0.461 (2)	0.705 (2)	0.503 (1)	0.66 (1)
	B [Å^2]	2.88 (7)	2.88[a]	2.88[a]	2.88[a]
Na_f (2b site)	Na [g]	0.208 (2)	0.294 (2)	0.166 (1)	0.30 (1)
	B [Å^2]	4.2 (1)	4.2[a]	4.2[a]	4.2[a]
Agreement factors					
R_{wp} [%]		9.447	14.172	10.517	6.992
R_p [%]		6.785	10.509	7.799	5.539
S		0.6067	1.2717	0.9388	0.8836

[a] These values are consistent with the pristine material and were not refined.

this irreversible structure change is continuing in the following cycles, the change in the crystal volume after thousands of electrochemical cycles will be serious although the initial irreversible change in crystal is very small. Based on the excellent cycle stability of this electrode material (Figure 2d), it is proposed that most of this small structural change occurs only during the initial Na^+ insertion into the fresh crystal structure, and that the structural changes during the following cycles are even smaller. The refined lattice parameters of sample 4 strongly support this proposition. After the Na^+ ions have been inserted/extracted into/from the crystal of P2-NCT for 500 cycles, the variations in the lengths of the *c* axis or the *a* (*b*) axis are still extremely small (compare samples 2 and 4), and the unit-cell volume has only decreased by 0.046%, indicating appealing crystal structure reversibility and a high stability of the P2-NCT material on sodium storage. The relatively large crystal-volume expansion during the initial Na^+ insertion process is possibly due to Na^+ reordering caused by the energy minimization mechanism between Na^+ and Na^+ when all 0.33 equivalents of the Na^+ ions are first inserted into the fresh P2-NCT material.[9]

The almost absent structural changes during cycling most likely result from the superior stability of the crystal structure and a maximum amount of 0.33 active Na^+ ions per formula of P2-NCT. Furthermore, it can be clearly seen from Table 1 that the occupancy variation of Na^+ ions is smaller at the Na_f position than at the Na_e position. After the electrode material had been cycled 500 times, the Na^+ occupancies of both the Na_f and Na_e positions with the same 0.15 V discharged state were almost identical for samples 2 and 4, illustrating the reversibility of sodium storage, which is useful to support the structure stability of P2-NCT during the Na^+ insertion/extraction processes. Furthermore, after 0.33 equivalents of Na^+ ions per formula had been inserted into the crystal during the initial discharge process, the layered character of the electrode material (sample 2) was also analyzed by HAADF/ABF STEM techniques: It was found that the typical P2-type structure was well preserved, and that two different Na^+ occupancies (Na_e and Na_f) can still be found (Figure S8). These results corroborate the structural stability of the P2-NCT materials, which will lead to an excellent cycle life (Figure 2d).

In conclusion, a $Na_{2/3}Co_{1/3}Ti_{2/3}O_2$ layered oxide with a pure P2-type structure (space group *P*63/*mmc*) was prepared by a solid-state reaction method. Excellent structural stability was observed during the sodium storage process. Even after 500 cycles of sodium insertion/extraction processes, the P2-type structure was still preserved, while new phases did not appear, and only a very small contraction of the volume of 0.046% was observed. This superior stable P2-type structure effectively ensures the electrochemical cycle stability of this material, which was used as the anode in NIBs. After 3000 cycles, the capacity retention still amounted to 84.84%; therefore, to the best of our knowledge, this materials displays the smallest capacity-decay rate (ca. 0.005%) reported for electrodes of NIBs. Furthermore, the good rate performance (ca. 41% of the reversible capacity were maintained even at a rate of 10C) and a reversible capacity of approximately 90 $mAh\,g^{-1}$ at a safe average storage voltage of about 0.7 V are also attractive features of this material and enable its use in NIBs. The simultaneous occupancy of Na_e and Na_f positions by the Na^+ ions was also revealed and confirmed by local structure analysis for the first time. These findings will speed up the development of room-temperature NIBs and advance the utilization of NIBs in large-scale energy-storage devices.

Received: April 22, 2014
Published online: June 24, 2014

Keywords: anode materials · electrochemistry · sodium-ion batteries · sodium storage

[1] a) B. Dunn, H. Kamath, J. M. Tarascon, *Science* **2011**, *334*, 928–935; b) M. Pasta, C. D. Wessells, R. A. Huggins, Y. Cui, *Nat. Commun.* **2012**, *3*, 1149.

[2] a) Y. S. Wang, X. Q. Yu, S. Y. Xu, J. M. Bai, R. J. Xiao, Y. S. Hu, H. Li, X. Q. Yang, L. Q. Chen, X. J. Huang, *Nat. Commun.* **2013**, *4*, 2365; b) N. Yabuuchi, M. Kajiyama, J. Iwatate, H. Nishikawa, S. Hitomi, R. Okuyama, R. Usui, Y. Yamada, S. Komaba, *Nat. Mater.* **2012**, *11*, 512–517; c) H. J. Yu, S. H. Guo, Y. B. Zhu, M. Ishida, H. S. Zhou, *Chem. Commun.* **2014**, *50*, 457–459.

[3] a) R. Berthelot, D. Carlier, C. Delmas, *Nat. Mater.* **2011**, *10*, 74–80; b) S. W. Kim, D. H. Seo, X. H. Ma, G. Ceder, K. Kang, *Adv. Energy Mater.* **2012**, *2*, 710–721; c) H. L. Pan, Y. S. Hu, L. Q. Chen, *Energy Environ. Sci.* **2013**, *6*, 2338–2360; d) M. D. Slater, D. Kim, E. Lee, C. S. Johnson, *Adv. Funct. Mater.* **2013**, *23*, 947–958; e) D. H. Lee, J. Xu, Y. S. Meng, *Phys. Chem. Chem. Phys.* **2013**, *15*, 3304–3312; f) L. Wang, Y. H. Lu, J. Liu, M. W. Xu, J. G. Cheng, D. W. Zhang, J. B. Goodenough, *Angew. Chem.* **2013**, *125*, 2018–2021; *Angew. Chem. Int. Ed.* **2013**, *52*, 1964–1967; g) S. Komaba, N. Yabuuchi, T. Nakayama, A. Ogata, T. Ishikawa, I. Nakai, *Inorg. Chem.* **2012**, *51*, 6211–6220; h) D. Kim, S. H. Kang, M. Slater, S. Rood, J. T. Vaughey, N. Karan, M. Balasubramanian, C. S. Johnson, *Adv. Energy Mater.* **2011**, *1*, 333–336; i) C. S. Park, H. Kim, R. A. Shakoor, E. Yang, S. Y. Lim, R. Kahraman, Y. Jung, J. W. Choi, *J. Am. Chem. Soc.* **2013**, *135*, 2787–2792; j) Y. L. Cao, L. F. Xiao, W. Wang, D. W. Choi, Z. M. Nie, J. G. Yu, L. V. Saraf, Z. G. Yang, J. Liu, *Adv. Mater.* **2011**, *23*, 3155–3160; k) V. L. Chevrier, G. Ceder, *J. Electrochem. Soc.* **2011**, *158*, A1011–A1014; l) Y.-U. Park, D.-H. Seo, H.-S. Kwon, B. Kim, J. Kim, H. Kim, I. Kim, H.-I. Yoo, K. Kang, *J. Am. Chem. Soc.* **2013**, *135*, 13870–13878; m) H. L. Chen, Q. Hao, O. Zivkovic, G. Hautier, L. S. Du, Y. Z. Tang, Y. Y. Hu, X. H. Ma, C. P. Grey, G. Ceder, *Chem. Mater.* **2013**, *25*, 2777–2786; n) J. F. Qian, M. Zhou, Y. L. Cao, X. P. Ai, H. X. Yang, *Adv. Energy Mater.* **2012**, *2*, 410–414; o) Y. You, X. L. Wu, Y. X. Yin, Y. G. Guo, *J. Mater. Chem. A* **2013**, *1*, 14061–14065; p) Y. You, X. L. Wu, Y. X. Yin, Y. G. Guo, *Energy Environ. Sci.* **2014**, *7*, 1643–1647; q) Y. Yan, Y.-X. Yin, Y.-G. Guo, L.-J. Wan, *Adv. Energy Mater.* **2014**, DOI: 10.1002/aenm.201301584.

[4] a) Z. L. Jian, W. Z. Han, X. Lu, H. X. Yang, Y. S. Hu, J. Zhou, Z. B. Zhou, J. Q. Li, W. Chen, D. F. Chen, L. Q. Chen, *Adv. Energy Mater.* **2013**, *3*, 156–160; b) K. Saravanan, C. W. Mason, A. Rudola, K. H. Wong, P. Balaya, *Adv. Energy Mater.* **2013**, *3*, 444–450.

[5] K.-H. Ha, S. H. Woo, D. Mok, N.-S. Choi, Y. Park, S. M. Oh, Y. Kim, J. Kim, J. Lee, L. F. Nazar, K. T. Lee, *Adv. Energy Mater.* **2013**, *3*, 770–776.

[6] a) S. Komaba, W. Murata, T. Ishikawa, N. Yabuuchi, T. Ozeki, T. Nakayama, A. Ogata, K. Gotoh, K. Fujiwara, *Adv. Funct. Mater.* **2011**, *21*, 3859–3867; b) H. L. Pan, X. Lu, X. Q. Yu, Y. S. Hu, H. Li, X. Q. Yang, L. Q. Chen, *Adv. Energy Mater.* **2013**, *3*, 1186–1194; c) A. Rudola, K. Saravanan, C. W. Mason, P. Balaya, *J.*

Mater. Chem. A **2013**, *1*, 2653 – 2662; d) M. Shirpour, J. Cabana, M. Doeff, *Energy Environ. Sci.* **2013**, *6*, 2538 – 2547; e) A. Darwiche, C. Marino, M. T. Sougrati, B. Fraisse, L. Stievano, L. Monconduit, *J. Am. Chem. Soc.* **2012**, *134*, 20805 – 20811; f) Y. Kim, Y. Park, A. Choi, N. S. Choi, J. Kim, J. Lee, J. H. Ryu, S. M. Oh, K. T. Lee, *Adv. Mater.* **2013**, *25*, 3045 – 3049.

[7] The P2 notation was proposed by Delmas et al. and refers to the ABBA stacking of the oxygen layer; see: C. Delmas, J. J. Braconnier, C. Fouassier, P. Hagenmuller, *Solid State Ionics* **1981**, *3 – 4*, 165 – 169.

[8] F. Izumi, K. Momma, *Solid State Phenom.* **2007**, *130*, 15 – 20.

[9] M. Roger, D. J. P. Morris, D. A. Tennant, M. J. Gutmann, J. P. Goff, J. U. Hoffmann, R. Feyerherm, E. Dudzik, D. Prabhakaran, A. T. Boothroyd, N. Shannon, B. Lake, P. P. Deen, *Nature* **2007**, *445*, 631 – 634.

[10] a) H. J. Yu, H. J. Kim, Y. R. Wang, P. He, D. Asakura, Y. Nakamura, H. S. Zhou, *Phys. Chem. Chem. Phys.* **2012**, *14*, 6584 – 6595; b) H. J. Yu, Y. M. Qian, M. R. Otani, D. M. Tang, S. H. Guo, Y. B. Zhu, H. S. Zhou, *Energy Environ. Sci.* **2014**, *7*, 1068 – 1078.

[11] N. Yabuuchi, K. Yoshii, S. T. Myung, I. Nakai, S. Komaba, *J. Am. Chem. Soc.* **2011**, *133*, 4404 – 4419.

